ORIGINAL RESEARCH ARTICLE

Leukocyte classification for acute lymphoblastic leukemia timely diagnosis by interpretable artificial neural network

Agnese Sbrollini, Selene Tomassini, Ruba Sharaan, Micaela Morettini, Aldo Franco Dragoni, Laura Burattini*

Department of Information Engineering, Università Politecnica delle Marche, Ancona 60121, Italy. E-mail: l.burattini@ univpm.com

ABSTRACT

Leukemia is a blood cancer characterized by leukocyte overproduction. Clinically, the reference for acute lymphoblastic leukemia diagnosis is a blood biopsy that allows obtain microscopic images of leukocytes, whose early-stage classification into leukemic (LEU) and healthy (HEA) may be disease predictor. Thus, the aim of this study is to propose an interpretable artificial neural network (ANN) for leukocyte classification to timely diagnose acute lymphoblastic leukemia. The "ALL_IDB2" dataset was used. It contains 260 microscopic images showing leukocytes acquired from 130 LEU and 130 HEA subjects. Each microscopic image shows a single leukocyte that was characterized by 8 morphological and 4 statistical features. An ANN was developed to distinguish microscopic images acquired from LEU and HEA subjects, considering 12 features as inputs and the local-interpretable model-agnostic explanatory (LIME) algorithm as an interpretable post-processing algorithm. The ANN was evaluated by the leave-one-out cross-validation procedure. The performance of our ANN is promising, presenting a testing area under the curve of the receiver operating characteristic equal to 87%. Being implemented using standard features and having LIME as a post-processing algorithm, it is clinically interpretable. Therefore, our ANN seems to be a reliable instrument for leukocyte classification to timely diagnose acute lymphoblastic leukemia, guaranteeing a high clinical interpretability level.

Keywords: Acute Lymphoblastic Leukemia; Artificial Neural Networks; Morphological and Statistical Features; Interpretability; LIME

1. Introduction

Leukocytes, commonly known as white blood cells, are a prime component of the immune system[1]. Leukemia is a type of blood cancer characterized by an excessive overproduction of leukocytes, which flood the bloodstream, crowd out healthy cells, and impede normal cell death[2]. Acute lymphoblastic leukemia is the most common blood neoplastic disease[3] (followed by acute myeloid leukemia, chronic lymphoblastic leukemia, and chronic myeloid leukemia), and its incidence ranges from 0.7 to 1.8/100,000 per year in adults[3,4]. Among the risk factors for developing acute lymphoblastic leukemia, the main ones are older age, exposure to oncological treatment, and genetic disorders[5]. The gold standard examinations for acute lymphoblastic leukemia diagnosis are complete blood count, peripheral blood smear, bone marrow analysis, and histochemical investigations. Thus, clinically, the reference for acute lymphoblastic leukemia diagnosis is blood biopsy, which allows to obtain microscopic images of leukocytes.

It is well known that the main evidence of acute lymphoblastic leukemia is the increased number of leukocytes. Thus, biologists and oncologists are used to visually count and characterize

these cells. Unfortunately, this practice is subjective, expensive, and time-consuming. If cells in the sample are insufficient or unavailable, patients are subjected to undergo further examinations. Moreover, the number of leukocytes is a reliable feature only during advanced stages of acute lymphoblastic leukemia[4], and, thus, not sufficient for a timely, safe, and accurate early-stage diagnosis. On the other hand, the single leukocyte characterization and classification into leukemic (LEU, **Figure 1(a)**) and healthy (HEA, **Figure 1(b)**) may be a predictor of acute lymphoblastic leukemia and a valid tool to investigate its natural progression and related symptoms. So, algorithms for the automatic characterization and classification of leukocytes from microscopic images are desirable.

In the literature, several automatic procedures have been proposed to detect and classify leukocytes[4,6–20]. Most of them focused on leukocyte detection by counting the number of cells[4,6–13], whereas only a small fraction aimed to classify leukocytes[14–20]. Focusing on leukocyte classification, the majority of automatic procedures are dealing with deep-learning methods[15,17,19,20] or advanced machine-learning classifiers[14,16,18] to improve classification accuracy. Despite the high performance, no method in the literature has specifically analyzed the clinically relevant features of single leukocytes that may lead to a preventive diagnosis of acute lymphoblastic leukemia. Thus, in this clinical scenario, interpretability is of crucial importance, as it allows to identify which are the most informative leucocyte features for acute lymphoblastic leukemia diagnosis and pathophysiology evaluation.

Thereby, the aim of this study is to propose a feature-based tool for leukocyte classification in order to timely diagnose acute lymphoblastic leukemia by an interpretable artificial neural network (ANN), guaranteeing a high level of clinical interpretability, usefulness, and practicability.

2. Materials and methods

2.1 Dataset

The publicly available "ALL_IDB: Acute Lymphoblastic Leukemia Image Database for Image Processing" database (https://scotti.di.unimi.it/all/) of Università di Milano[21–24] was considered. It is made up of two datasets "ALL_IDB1" and "ALL_

IDB2". In this study, the "ALL_IDB2" dataset was used, as it considers microscopic images with single leukocytes. Indeed, the "ALL_IDB2" dataset consists of 260 microscopic images showing leukocytes acquired from 130 LEU and 130 HEA subjects. Microscopic images were captured by an optical laboratory microscope coupled with a Canon PowerShot G5 camera. They were acquired with a resolution of 257 pixels × 257 pixels and stored in ".jpg" format, according to 24-bit RGB color depth.
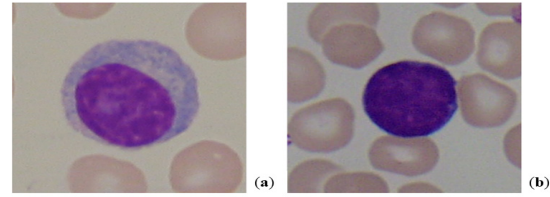

Figure 1. Microscopic images showing leukocytes of LEU (a) and HEA (b) subjects.

2.2 Artificial neural network construction

2.2.1 Preprocessing

Firstly, each microscopic image was prefiltered. **Figure 2** depicts the preprocessing outcomes of one microscopic image acquired from a subject affected by leukemia (**Figure 2(a)**). Specifically, grayscale conversion (**Figure 2(b)**), contrast enhancement (**Figure 2(c)**), and image complement (**Figure 2(d)**) were applied to improve visibility and reduce noise. Then, a binary image was obtained by applying an automated threshold equal to 0.5. From each binary image, a single leukocyte was selected and, then, extracted as the white area larger than 1,000 pixels (**Figure 2(e)**). According to the binary images, every single leukocyte was segmented (**Figure 2(f)**).

2.2.2 Feature extraction

Each segmented leukocyte was characterized by 8 morphological and 4 statistical features. Morphological features, selected according to hematologists' experience[10], are:

• minor axis length (mAL, pixels), computed as the length of the minor axis of the ellipse that has the same normalized second central moments as the segmented leukocyte;

• major axis length (MAL, pixels), computed as the length of the major axis of the ellipse that has
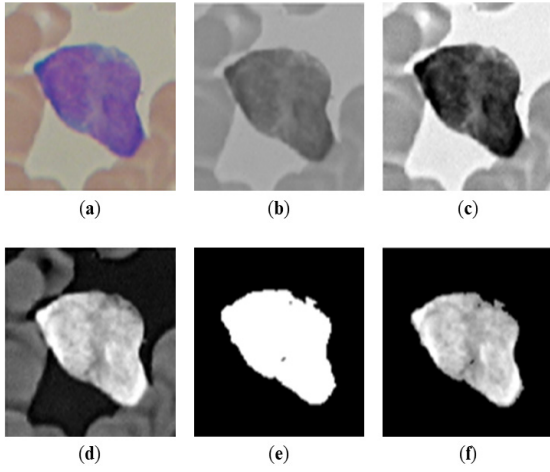
2

Figure 2. Preprocessing outcomes of one microscopic image acquired from a subject affected by leukemia: (a) raw image; (b) grayscale image; (c) contrast enhanced image; (d) complement image; (e) binary image; and (f) segmented image.

the same normalized second central moments as the segmented leukocyte;

• perimeter (PER, pixels), computed as the distance between each adjoining pair of pixels around the border of the segmented leukocyte;

• area (AR, pixels^2), computed as the number of pixels that composed the segmented leukocyte;

• solidity (SOL, adi), computed as the ratio of actual area and the convex hull area that composed the segmented leukocyte;

• eccentricity (ECC, adi), computed as the ratio of the distance between the foci of the ellipse that has the same normalized second central moments as the segmented leukocyte and MAL;

• form factor (FF, adi), computed as:

$$FF = \frac{4 \times \pi \times AR}{PER^2}$$

(1)

• compactness (COM, adi), computed as:

$$COM = \frac{PER^2}{AR}$$

(2)

Statistical features are:

• contrast (CON, adi), computed as the intensity contrast between a pixel and its neighbor over the segmented leukocyte;

• correlation (COR, adi), computed as the correlation contrast between a pixel and its neighbor over the segmented leukocyte;

• energy (EN, adi), computed as the sum of squared elements between a pixel and its neighbor over the segmented leukocyte;

• homogeneity (HOM, adi), computed as the closeness between a pixel and its neighbor over the

segmented leukocyte.

2.2.3 Artificial neural network

The classification was performed to distinguish microscopic images acquired from LEU and HEA subjects. Our ANN was designed with 12 inputs, corresponding to the number of features, and an output layer, corresponding to LEU/HEA classification. Thus, ANN presents twelve neurons in the inner layer, one neuron in the out layer, and one hidden layer. The number of neurons in the hidden layer was selected during the validation process (as described below). All neurons were initialized by random weights and biases (ranging between −1 and +1) and characterized by a sigmoid activation function. ANN was trained according to the Levenberg-Marquardt optimization backpropagation algorithm and the early-stop validation criterion was employed to prevent overfitting[25]. Local-interpretable model-agnostic explanatory (LIME) algorithm[26] was applied as an interpretable post-processing algorithm. LIME is an explainer algorithm able to interpret ANN predictions by combining features and coefficients of such trained ANN. It locally approximates the ANN with an interpretable model, ranking ANN inputs according to their impact on classification performance.

ANN was evaluated by the leave-one-out cross-validation procedure, a kind of k-fold cross-validation that considers k equal to the number of instances in the dataset. Specifically, for each fold, ANN was trained by using a training set, composed of k-1 instances, and tested on the remaining instance. At the end of the leave-one-out cross-validation procedure, ANN was trained on k training sets and tested on a testing set composed of the k remaining instances of each k fold. Leave-one-out cross-validation procedure was repeated in order to select ANN architecture by varying the number of neurons in the hidden layer from 100 to 500. The ANN providing the highest median value of the areas under the curve (AUC) of the receiver operating characteristic (ROC) curves of k training sets was selected.

2.3 Statistics

Feature distribution normality was evaluated by the Lilliefors test. Feature comparison between LEU and HEA subjects was performed by unpaired Wilcoxon rank-sum test.

3

ANN performance was evaluated by ROC and confusion matrix analysis, considering both training sets and testing set obtained by the leave-one-out cross-validation procedure. ROC was characterized by computing the AUC. The confusion matrix was constructed by computing the number of true positives (TP, number of LEU leukocytes classified as LEU), true negatives (TN, number of HEA leukocytes classified as HEA), false negatives (FN, number of LEU leukocytes classified as HEA) and false positives (FP, number of HEA leukocytes classified as LEU). Values of sensitivity (SE), specificity (SP), and accuracy (AC) were computed according to the following formulae:

$$SE = \frac{TP}{TP + FN} \tag{3}$$

$$SP = \frac{TN}{TN + FP} \tag{4}$$

$$AC = \frac{TP + TN}{TP + TN + FP + FN} \tag{5}$$

Interpretation of each feature was assessed by univariate AUC and feature relevance (FR) criteria considering the entire dataset. FR of each feature was assessed by processing the feature ranking obtained by LIME. Thus, for each subject, a feature ranking was constructed by analysis of the coefficients of the selected ANN. FR is the weighted average (by ranking) of the percentage of patients presenting a specific feature in each of the ranking positions. The association between feature-interpretation criteria was assessed by Spearman's correlation analysis (ρ). Non-normal distributions were reported as 50th (median) [25th; 75th] percentiles. The statistical significance level (P-value) was set at 0.05.

3. Results

Table 1 reports feature distributions of LEU and HEA and comparisons. According to the results, 6 out of 8 distributions of morphological features (mAL, MAL, AR, SOL, FF and COM) and 2 out of 4 distributions of statistical features (CON and COR) of LEU leukocytes are statistically (P-value < 0.05) different from features of HEA leukocytes.

Figure 3 depicts the selected ANN and the feature importance quantified by both univariate AUC and FR criteria. The selected ANN has 135 neurons in the only hidden layer. **Figure 4** depicts the ROC curve of ANN by considering all training sets (**Figure 4(a)**) and testing sets (**Figure 4(b)**) obtained from the leave-one-out cross-validation procedure. ANN performance provided by ROC and confusion matrix analysis for both training sets and testing set is very promising, as reported in **Table 2**.

Feature importance quantified by univariate AUC and FR criteria is reported in **Table 3**. Specifically, according to the univariate AUC criterion, the feature with the highest importance is AR (univariate AUC = 69.29%), whereas the worst is HOM (univariate AUC = 50.94%). According to the FR criterion, the feature with the highest importance is AR (FR = 14.44%), whereas the worst is EN (FR = 2.15%). Despite the Spearman's correlation between the two criteria is low and not statistically significant (ρ = 0.23, P-value = 0.47), morphological features have high-ranking positions in both univariate AUC and FR criteria (e.g., AR is in the first position in both criteria) and statistical features have low ranking positions in both univariate AUC and FR criteria (e.g., HOM is in the last position according to univariate AUC criterion, and EN is in the last position according to FR criterion).

Table 1. Non-normal distributions of features extracted from images acquired from LEU and HEA subjects are reported as 50th (median) [25th; 75th] percentiles. Feature comparison was performed by unpaired Wilcoxon rank-sum test

		LEU	HEA	*P*-value
Morphological features	mAL (pixels)	106.33* [94.76; 118.30]	96.94 [80.67; 106.13]	$< 10^{-4}$
	MAL (pixels)	125.86* [112.70; 144.09]	117.92 [98.03; 141.37]	< 0.01
	PER (pixels)	385.71 [349.42; 465.93]	374.78 [311.77; 472.01]	0.13
	AR (pixels^2)	9,910* [8,516; 13,005]	8,582 [5,926; 9,979]	$< 10^{-7}$
	SOL (adi)	0.97* [0.94; 0.98]	0.94 [0.81; 0.97]	$< 10^{-6}$
	ECC (adi)	0.53 [0.40; 0.67]	0.58 [0.44; 0.71]	0.12
	FF (adi)	0.81* [0.52; 0.91]	0.72 [0.32; 0.87]	< 0.01
	COM (adi)	14.02* [12.82; 16.29]	15.46 [13.89; 20.42]	$< 10^{-4}$
Statistical features	CON (adi)	0.30* [0.28; 0.33]	0.32 [0.30; 0.43]	$< 10^{-4}$
	COR (adi)	0.98* [0.98; 0.98]	0.98 [0.98; 0.98]	< 0.05
	EN (adi)	0.24 [0.21; 0.29]	0.27 [0.22; 0.30]	0.13
	HOM (adi)	0.92 [0.91; 0.93]	0.92 [0.91; 0.93]	0.79

Table 2. ANN performance provided by ROC and confusion matrix analysis for both training sets and testing set

	AUC (%)	TP	TN	FN	FP	SE (%)	SP (%)	AC (%)
Training sets	94 [93; 95]	117 [114; 120]	113 [104; 119]	17 [11; 25]	12 [9; 16]	87 [82; 91]	90 [88; 92]	88 [85; 90]
Testing set	87	110	101	29	20	79	83	81

Table 3. Feature importance (ranking-values) quantified by univariate AUC and FR criteria

		Univariate AUC	FR
Morphological features	mAL (pixels)	4–65.21%	4–1.84%
	MAL (pixels)	7–59.90%	3–12.74%
	PER (pixels)	11–55.37%	2–13.89%
	AR (pixels^2)	1–69.29%	1–14.44%
	SOL (adi)	2–68.53%	7–6.82%
	ECC (adi)	9–55.64%	10–4.55%
	FF (adi)	6–60.89%	9–5.44%
	COM (adi)	5–64.98%	5–10.66%
Statistical features	CON (adi)	3–65.79%	11–3.07%
	COR (adi)	8–59.18%	6–7.90%
	EN (adi)	10–55.47%	12–2.15%
	HOM (adi)	12–50.94%	8–6.50%
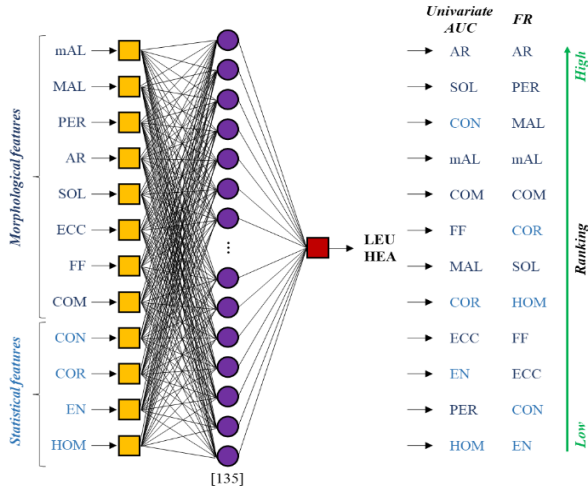
Figure 3. Selected ANN (135 neurons in the only hidden layers) and feature importance quantified by both univariate AUC and FR criteria.
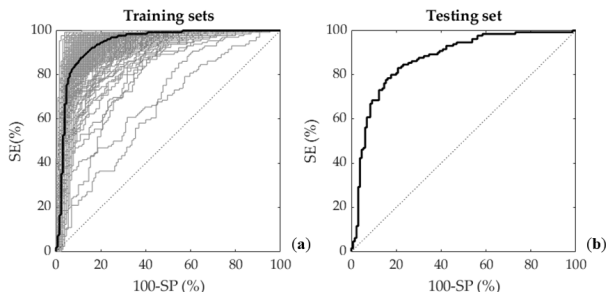
Figure 4. ROC curve of ANN obtained from the leave-one-out cross-validation procedure: (a) depicts results of training sets (in gray) and their median value (in black), whereas (b) depicts results of testing set.

4. Discussion

The aim of this study was to develop a novel instrument for leukocyte classification by interpretable artificial neural network in order to timely diagnose acute lymphoblastic leukemia, guaranteeing high level of clinical interpretability. To this aim, microscopic images of leukemic and healthy leukocytes were analyzed.

In clinics, it is well known that leukocyte number and their multiparameter characterization are indicators of acute lymphoblastic leukemia, but not specific for an early-stage diagnosis. To fulfill a timely intervention on disease progression, prevention actions are essential. To do so, instruments able to capture even the slightest leukocyte alterations, acting like precursors of acute lymphoblastic leukemia, are desirable. Hence, the here proposed study focused on processing only microscopic images containing single leukocytes.

To obtain more information regarding the natural progression of the disease and provide timely therapeutic intervention, clinical interpretability should be ensured. Thus, our automatic instrument works with both morphological and statistical features of leukocytes, generally known and used by biologists and oncologists for the leukocyte characterization of leukemic subjects.

Considering our results, the best features for discriminating leukemic from healthy leucocytes are morphological features (in particular, the morphological area of leukocytes), as confirmed also by results provided by feature-importance comparison. This outcome is encouraging because morphological features are clinically interpretable better than statistical ones and, consequently, more usable in

the real clinical scenario.

However, none of the considered features provided high performance in terms of leukocyte classification, as demonstrated by univariate area under the curve of the single features. Thus, advanced methods for feature combination are pivotal. To combine both morphological and statistical features of single leukocytes, an artificial neural network was implemented. The settings of our artificial neural network were selected on the basis of a robustness analysis (by varying the number of neurons), whereas its generalization property was evaluated by cross-validation. The results of our artificial neural network are very promising (testing area under the curve of the receiver operating characteristic equal to 87%), also in terms of sensitivity (79%) and specificity (83%). Moreover, our artificial neural network is robust in terms of performance, as demonstrated by the narrow confidence intervals of the training area under the curve of the receiver operating characteristic (2%) provided by the cross-validation procedure. This result highlights the reliability of the entire algorithm and the robustness of the proposed method on training data, a property that makes our artificial neural network an effective tool to generalize clinical acute lymphoblastic leukemia diagnosis in the real clinical scenario.

In the literature, several automatic procedures have been proposed to classify leukocytes (**Table 4**). Among the studies leveraging on leukocyte classification, six of them considered the dataset "ALL_IDB2" of the publicly available "ALL_IDB: Acute lymphoblastic leukemia image database for image processing" database (https://scotti.di.unimi.it/all/) of Università di Milano[21–24]. Two out of six[15,16] extracted features from microscopic images of leukocytes, but none of them considered either an artificial neural network (one applied a chronological sine cosine algorithm-based convolutional neural network, the other used extra trees as a classifier) or the leave-one-out cross-validation strategy. Four out of six[17–20] classified the leukocytes by applying machine-learning and deep-learning methods, considering microscopic images as inputs (three used a convolutional neural network and one used a support vector machine as classifier). These studies validated the algorithms by using the k-fold cross-validation strategy or static data division in training and test sets. None of these six studies applied a correlation between the statistical relevance of features and the interpretability of the machine-learning tool. Only one out of the six[20] applied Grad-CAM as interpretable explainer, but not correlating its outputs with features usually evaluated by clinicians. Differently from the literature, our artificial neural network uses clinically interpretable features as inputs, the leave-one-out cross-validation strategy and LIME as interpretable post-processing algorithm.

Leave-one-out cross-validation is known to be a robust validation technique in case of small-sized datasets and independent from data splits, differently from the static data division. Considering the

Table 4. State-of-the-art automatic procedures for leukocyte classification using the "ALL_IDB2" dataset

Ref.	Input	Preprocessing	Classifier	Validation	Results	Interpretability
[15]	Features	Resizing	Chronological sine cosine algorithm-based convolutional neural network	k-fold cross validation (with k variable)	AC = 98.7%	No
[16]	Features	Resampling + resizing + data augmentation	Extra trees	k-fold cross validation (with k = 5)	AC = 96.2%	No
[17]	Images	Resizing + data augmentation	Convolutional neural network	k-fold cross validation (with k = 10)	AC = 97.2%	No
[18]	Images	Data augmentation	Support vector machine	k-fold cross validation (with k = 5)	AC = 94.2%	No
[19]	Images	Resizing	Convolutional neural network	Static data division (70% training, 30% test)	AC = 99.1%	No
[20]	Images	Color normalization + greyscale conversion + binarization + data augmentation	Convolutional neural network	k-fold cross-validation (with k = 2) repeated 10 times	AC = 96.8%	Yes (Grad-CAM), heatmap
Proposed study	Features	Grayscale conversion + contrast enhancement + complement + binarization	Artificial neural network	Leave-one-out cross validation	AC = 81.0%	Yes (LIME), feature relevance

importance of association between the well-known statistical relevance of features and the interpretable performance of machine-learning methods, our artificial neural network guarantees a transparent correspondence between input features and interpretable outputs of LIME. Indeed, our artificial neural network confirmed the importance of morphological features (in particular, the morphological area of leukocytes) in detecting acute lymphoblastic leukemia, as widely confirmed by the literature and the statistical approaches. This property makes our approach suitable to be used in the real clinical scenario, despite it has not the highest performance in term of sensitivity, specificity, and accuracy.

Of course, our approach can be improved. Firstly, the computed features refer uniquely to grayscale converted microscopic images, instead of using raw RGB colormap. Moreover, advanced visualization modules for machine-learning tools were presented to highlight the pattern that influenced the automatic decision-making process the most. However, our approach considers only statistical analysis as feature clinical interpretation, without being assessed by biologists or oncologists. Expert revision of cases would be essential to define novel additional features that can be inserted as inputs of our artificial neural network and, consequently, to improve the performance of our tool, specifically in terms of clinical sensitivity. Finally, the used database includes uniquely leukocyte classification into leukemic and healthy, without considering microscopic images of leukemic leukocytes collected during different stages of acute lymphoblastic leukemia or microscopic images of leukocytes collected in patients affected by white blood cell disorders. These additional data may reveal specific features of leukemic leukocytes and, thus, help to refine our tool and to improve the performance of our tool, specifically in terms of clinical specificity. Therefore, future studies will investigate the possibility to improve our artificial neural network, both technically and clinically. Specifically, implementation of colormap-based features and advanced visualization techniques for machine-learning understanding will improve the performance of the algorithm, while clinical feedback from our biological/medical partners and integration of additional databases will improve the interpretability and scalability of clinical scenarios, considering the seriousness of the disease.

5. Conclusion

Our artificial neural network seems to be a reliable instrument for leukocyte classification in order to timely diagnose acute lymphoblastic leukemia, ensuring high level of clinical interpretability.

Author contributions

Conceptualization, AS, ST and RS; methodology, AS and ST; software, AS, ST and RS; validation, AS and ST; formal analysis, AS and ST; investigation, AS, ST and RS; resources, LB; data curation, RS; writing—original draft preparation, AS and ST; writing—review and editing, AS, ST, RS, MM, AFD and LB; visualization, AS and ST; supervision, LB; project administration, LB; funding acquisition, MM, AFD and LB.

Acknowledgments

Conflict of interest

No conflict of interest was reported by all authors.

References

1. Shah A, Naqvi SS, Naveed K, *et al*. Automated diagnosis of leukemia: A comprehensive review. IEEE Access 2021; 9: 132097–132124. doi: 10.1109/ACCESS.2021.3114059.

2. Parks PJ. Leukemia (compact research series). San Diego: ReferencePoint Press; 2010.

3. Litin SC. Mayo clinic family health book. 5th ed. Rochester: Mayo Clinic Press; 2018.

4. Fatonah NS, Tjandrasa H, Fatichah C. Identification of acute lymphoblastic leukemia subtypes in touching cells based on enhanced edge detection. International Journal of Intelligent Engineering and Systems 2020; 13: 204–215. doi: 10.22266/IJIES2020.0831.18.

5. Brown PA, Shah B, Advani A, *et al*. Acute lymphoblastic leukemia, version 2.2021, NCCN clinical practice guidelines in oncology. Journal of the National Comprehensive Cancer Network 2021; 19(9): 1079–1109. doi: 10.6004/jnccn.2021.0042.

6. Bibi N, Sikandar M, Ud Din I, *et al*. IoMT-based automated detection and classification of leukemia

using deep learning. Journal of Healthcare Engineering 2020; 2020: 1–12. doi: 10.1155/2020/6648574.

7. Hamza MA, Albraikan AA, Alzahrani JS, *et al.* Optimal deep transfer learning-based human-centric biomedical diagnosis for acute lymphoblastic leukemia detection. Computational Intelligence and Neuroscience 2022; 2022: 1–13. doi: 10.1155/2022/7954111.

8. Kumar A, Rawat J, Kumar I, *et al.* Computer-aided deep learning model for identification of lymphoblast cell using microscopic leukocyte images. Expert Systems 2022; 39: e12894. doi: 10.1111/exsy.12894.

9. Umamaheswari D, Geetha S. Fuzzy-C means segmentation of lymphocytes for the identification of the differential counting of WBC. International Journal of Cloud Computing 2021; 10: 26–42. doi: 10.1504/IJCC.2021.113974.

10. Bodzas A, Kodytek P, Zidek J. Automated detection of acute lymphoblastic leukemia from microscopic images based on human visual perception. Frontiers in Bioengineering and Biotechnology 2020; 8: 1005. doi: 10.3389/fbioe.2020.01005.

11. Abdulla AA. Efficient computer-aided diagnosis technique for leukaemia cancer detection. IET Image Processing 2020; 14(17): 4435–4440. doi: 10.1049/iet-ipr.2020.0978.

12. Mohammed ZF, Abdulla AA. An efficient CAD system for ALL cell identification from microscopic blood images. Multimedia Tools and Applications 2021; 80: 6355–6368. doi: 10.1007/s11042-020-10066-6.

13. Das BK, Dutta HS. GFNB: Gini index-based fuzzy naive bayes and blast cell segmentation for leukemia detection using multi-cell blood smear images. Medical & Biological Engineering & Computing 2020; 58: 2789–2803. doi: 10.1007/s11517-020-02249-y.

14. Putzu L, Caocci G, Di Ruberto C. Leucocyte classification for leukaemia detection using image processing techniques. Artificial Intelligence in Medicine 2014; 62(3): 179–191. doi: 10.1016/j.artmed.2014.09.002.

15. Jha KK, Dutta HS. Mutual information based hybrid model and deep learning for acute lymphocytic leukemia detection in single cell blood smear images. Computer Methods and Programs in Biomedicine 2019; 179: 104987. doi: 10.1016/j.cmpb.2019.104987.

16. Rastogi P, Khanna K, Singh V. LeuFeatx: Deep learning-based feature extractor for the diagnosis of acute leukemia from microscopic images of peripheral blood smear. Computers in Biology and Medicine 2022; 142: 105236. doi: 10.1016/j.compbiomed.

17. Das PK, Meher S. An efficient deep convolutional neural network based detection and classification of acute lymphoblastic leukemia. Expert Systems with Applications 2021; 183: 115311. doi: 10.1016/j.eswa.2021.115311.

18. Vogado L, Veras R, Aires K, *et al.* Diagnosis of leukaemia in blood slides based on a fine-tuned and highly generalizable deep learning model. Sensors (Basel) 2021; 21(9): 2989. doi: 10.3390/s21092989.

19. Safuan SNM, Tomari MRM, Zakaria WNW, *et al.* Investigation of white blood cell biomarker model for acute lymphoblastic leukemia detection based on convolutional neural network. Bulletin of Electrical Engineering and Informatics 2020; 9(2): 611–618. doi: 10.11591/EEI.V9I2.1857.

20. Genovese A, Hosseini MS, Piuri V, *et al.* Acute lymphoblastic leukemia detection based on adaptive unsharpening and deep learning. In: Proceedings of 2021–2021 IEEE International Conference on Acoustics, Speech and Signal Processing (ICASSP); 2021 Jun 6–11; Toronto. New York: IEEE; 2021. p. 1205–1209.

21. Scotti F. Automatic morphological analysis for acute leukemia identification in peripheral blood microscope images. In: Proceedings of 2005 IEEE International Conference on Computational Intelligence for Measurement Systems and Applications; 2005 Jul 20–22; Messian. New York: IEEE; 2005. p. 96–101.

22. Piuri V, Scotti F. Morphological classification of blood leucocytes by microscope images. In: Proceedings of 2004 IEEE International Conference on Computational Intelligence for Measurement Systems and Applications; 2004 Jul 14–16; Boston. New York: IEEE; 2004. p. 103–108.

23. Labati RD, Piuri V, Scotti F. All_IDB: The acute lymphoblastic leukemia image database for image processing. In: Proceedings of 2011 18th IEEE International Conference on Image Processing; 2011 Sep 11–14; Brussels. New York: IEEE; 2011. p. 2045–2048.

24. Scotti F. Robust segmentation and measurements techniques of white cells in blood microscope images. In: Proceedings of 2006 IEEE Instrumentation and Measurement Technology Conference; 2006 Apr 24–27; Sorrento. New York: IEEE; 2006. p. 43–48.

25. Prechelt L. Early stopping—but when? In: Lecture notes in computer science. Heidelberg: Springer; 2012. p. 53–67.

26. Ribeiro MT, Singh S, Guestrin C. Why should I

trust you? In: Proceedings of the 22nd ACM SIG-KDD International Conference on Knowledge Discovery and Data Mining; 2016 Aug 13–17; San Francisco. New York: Association for Computing Machinery; 2016. p. 1135–1144.